

## Moving spatial solitons in active nonlinear-optical resonators

K. Staliunas, V. B. Taranenکو,\* G. Slekyس, R. Viselga, and C. O. Weiss  
*Physikalisch Technische Bundesanstalt, 38116 Braunschweig, Germany*  
 (Received 17 July 1997)

We investigate spatial solitons in a resonator with a narrow-band gain element and a saturable absorber placed in Fourier-conjugated resonator planes. Solitons are stationary or move at discrete velocities depending on the resonator tuning. The modulus of the velocity of moving solitons is fixed, but the direction of their motion is arbitrary. Solitons compete in velocity space. The experiments are conducted on a photorefractive oscillator with bacteriorhodopsin saturable absorber. Observations agree well with solutions of a general order parameter equation for such resonators. [S1050-2947(98)02701-2]

PACS number(s): 42.65.Sf, 42.60.Mi, 42.65.Tg

### I. INTRODUCTION

We show dynamical (moving) spatial solitons in a self-imaging resonator with a narrow-band gain element and a saturable absorber placed in Fourier-conjugated planes of the resonator. The gain element in our experiments is a photorefractive BaTiO<sub>3</sub> crystal placed in the far-field plane of the resonator and the saturable absorber is a bacteriorhodopsin (BR) cell placed in the near-field plane.

A similar system (with a self-imaging resonator and the nonlinear media in Fourier-conjugated planes) has been described in [1–3], where the existence of stationary spatial solitons was shown. In [1,2] a laser with saturable absorber was used and in [3] a system was studied where the gain and loss elements were differently oriented photorefractive crystals. The spatial solitons found in [1–3] are bistable, i.e., they can be “written” anywhere in the laser cross section. If subjected to extrinsic forces (e.g., phase gradients due to non-planar or tilted resonator mirrors, or gain gradients due to a spatially inhomogeneous pump), the soliton can move. The solitons in [1–3] are, however, stationary for transversally homogeneous parameters. In the present paper we show dynamical spatial solitons, which, differently from [1–3], move at discrete velocities for homogeneous laser parameters, with the velocity modulus depending on the resonator tuning and the direction of motion arbitrary.

The essential difference here from the experiments [1,2] is a narrow spectral line of the gain medium. In [1,2] a broadband laser medium was used, which causes no frequency selection and consequently no tunability of transverse modes (or transverse wave numbers). An aperture in the far-field plane was necessary for soliton stability. The spatial width of the solitons was determined by the inverse width of this aperture in [1,2]. Here we use a photorefractive crystal as the amplifying medium, which is equivalent to a narrow spectral gain line laser amplifier [4]. The width of the gain line [which for a photorefractive oscillator (PRO) is inversely proportional to the photon lifetime in the resonator [4]] is a fraction of free spectral range. This narrow gain line of the PRO amplifier allows spatial frequency selection in

addition to that caused by the aperture in the far-field plane. This narrow gain line PRO with zero resonator detuning is equivalent to the laser system with an aperture in the far-field plane and allows one to reproduce the results from [1,2]. On the other hand, the frequency-detuned narrow gain line PRO selects higher-order transverse modes or higher spatial frequencies, which leads to moving spatial solitons, as we show below.

The experimental scheme used in [3] seemingly could allow one to obtain moving spatial solitons too. The narrow gain PRO used in [3] is identical to our scheme as regards macroscopic physics. However, the intrinsic motion of solitons was not reported in [3].

### II. RESONATORS WITH NARROW-BAND GAIN

For a theoretical analysis we use model equations for resonators with a narrow-band gain element and saturable absorber, without specifying a particular nonlinear optical system. Two essential properties of the system are taken into account: (i) the self-imaging resonator and (ii) the amplifying medium and saturable absorber are placed in Fourier-conjugated planes of the resonator. The model equation for resonators with narrow-band gain is a complex Swift-Hohenberg equation (CSHE), which was derived for lasers in [5,6], for PROs in [4], and for optical parametric oscillators in [7]. For an additional saturable absorber, the nonlinearities in the CSHE are correspondingly modified [2].

For the experiments a ring resonator PRO with four highly reflecting plane mirrors and four identical intracavity lenses (focal length  $f=100$  mm) arranged in near-self-imaging geometry was used. The total length of the resonator is  $L=8f+l$ , where  $l$  is a small shift from the self-imaging configuration ( $|l|\ll f$ ). A BaTiO<sub>3</sub> crystal homogeneously pumped by a single frequency Ar<sup>+</sup> laser (514 nm) and a cell (with 10 mm diameter of aperture) of bacteriorhodopsin saturable absorber [8] (saturation intensity  $\sim 10$  mW/cm<sup>2</sup>) were placed in Fourier-conjugated planes of the resonator. The transverse structure of the PRO emission in the near field (saturable absorber plane) and in the far field (gain crystal plane) is monitored by a charge coupled device camera.

The PRO with an unbleached BR absorber was below threshold at maximum available pump intensity ( $\geq 120$  mW/cm<sup>2</sup>). The PRO emission was initiated by an

\*Permanent address: Institute of Physics National Academy of Sciences of the Ukraine, Kiev, Ukraine.

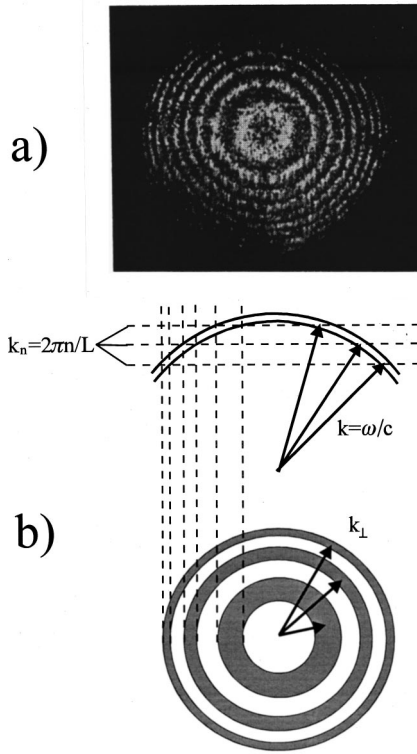


FIG. 1. (a) Far-field emission of PRO with the saturable absorber bleached. (b) Illustration of resonant rings in the far field of a planar resonator. The central frequency of the gain line determines the modulus of the wave vector  $k = \omega/c$ . The resonance condition determines the component of the wave vector along the optical axis  $k_{\parallel} = 2\pi n/l$ . Concentric resonant rings result with  $k_{\perp, n} \approx k - k_n^2/2k$ . Each ring corresponds to a different longitudinal mode family (with index  $n$ ). The width of the rings corresponds to the spectral width of the gain line.

additional (bleaching) expanded beam of a Nd:YAG laser (532 nm) (where YAG denotes yttrium aluminum garnet), which irradiated the BR absorber. The threshold for the oscillation onset was thus lowered to a few  $\text{mW}/\text{cm}^2$  of pump intensity. At relatively high pump intensities (20–30  $\text{mW}/\text{cm}^2$ ) dynamical transverse patterns, resembling speckle fields, are observed in the near-field plane. In the far field this corresponds to radiation on many resonant rings, as shown in Fig. 1(a).

The excitation of multiple resonant rings can be understood by employing the analogy between the plane mirror and self-imaging resonators. As shown recently [2,9], the near self-imaging resonator with a small shift  $l$  from self-imaging configuration is equivalent to the plane mirror resonator of total length  $l$ . Then the resonant frequencies of the equivalent plane mirror resonator are  $\omega_n = 2\pi c n/l$  and the resonant wave numbers  $k_n = 2\pi n/l$ . If the central frequency of the gain line  $\omega = kc$  does not coincide with any of resonant frequencies then one can decompose the wave vector  $\vec{k}$  (of arbitrary direction and fixed modulus  $k = \omega/c$ ) into longitudinal (parallel to resonator axis) and transverse components, as illustrated in Fig. 1(b). The longitudinal component must match the resonance condition of the cavity. The transversal component is then  $k_{\perp, n} = \sqrt{k^2 - k_n^2} \approx k - k_n^2/2k$ . This corresponds to a family of resonant rings in transverse wave

vector  $\vec{k}_{\perp}$  space, where each ring corresponds to one longitudinal mode family.

The emission on many longitudinal modes (many resonance rings) is not describable with the mean-field CSHE model, which by definition describes only a single longitudinal mode case. The CSHE describes the spatiotemporal dynamics of an order parameter  $A(\vec{r}_{\perp}, t)$ , which is proportional to the complex envelope of the optical field and is defined in the transverse plane  $\vec{r}_{\perp} = (x, y)$ :

$$\partial A / \partial t = (p - 1)A + i(\Delta + d\vec{\nabla}_{\perp}^2)A - \frac{(\Delta + d\vec{\nabla}_{\perp}^2)}{\Delta\omega^2} A - |A|^2 A. \quad (1)$$

Here  $\Delta$  is the resonator detuning,  $d = l\lambda Q/2\pi$  is the diffraction coefficient,  $l$  is the difference of the resonator length from the self-imaging length (or the total length of the corresponding plane mirror resonator),  $Q$  is the finesse of resonator,  $\lambda$  is the wavelength,  $p$  is the pump normalized to its threshold value, and  $\Delta\omega$  is the width of the gain line. (For the laser  $\Delta\omega$  corresponds to the width of the gain line; for PROs  $\Delta\omega = 2$  since the PRO gain line width is the width of the resonator mode line [4].) The Laplace operator acts in the near-field transverse plane  $\vec{\nabla}_{\perp}^2 = \partial^2/\partial x^2 + \partial^2/\partial y^2$ . The time in Eq. (1) is normalized to the characteristic relaxation time of the active resonator (photon lifetime in lasers or relaxation time of refractive index grating in PROs). The frequency is normalized to the corresponding relaxation rate.

It follows from Eq. (1) that the PRO supports waves with particular transverse wave numbers. Inserting the ansatz in the form of tilted waves  $A(\vec{r}_{\perp}, t) = \exp[\lambda(\vec{k}_{\perp})t + i\vec{k}_{\perp}\vec{r}_{\perp}]$  into Eq. (1), one obtains the form of the gain line  $\lambda(k_{\perp}) = p - 1 - (\Delta - dk_{\perp}^2)/\Delta\omega^2$ . Zero detuning leads to  $\lambda(k_{\perp}) = p - 1 - d^2 k_{\perp}^4/\Delta\omega^2$ , which corresponds to the action of the aperture in the far field (suppression of the higher components of the spatial spectrum). Nonzero detuning leads to maximum amplification of radiation with nonzero transverse wave numbers  $dk_{\perp}^2 = \Delta$ . In  $\vec{k}_{\perp}$  space the maximally amplified wave numbers lie on a ring with a radius proportional to detuning and a width proportional to the width of the gain line  $\Delta\omega$ . Consequently, PROs (and, in general, narrow gain line nonlinear optical systems) emit tilted waves, with the tilt angle proportional to the (positive) detuning. This has been shown for lasers in [10].

The theoretical approach (1) takes into account only one resonant ring (or the central spot, to which the ring contracts in the limit of zero detuning) since the mean-field approximation (single longitudinal mode) is assumed. In reality, with no external spatial frequency filtering an infinite number of rings is possible (Fig. 1). We used therefore a diaphragm in the far-field plane to restrict to only one ring.

The role of the diaphragm in our experiments is different from that in [1–3]. In [1–3] the radius of the diaphragm determined uniquely the size of the spot in the Fourier plane and consequently the width of the soliton beam. In our case of a narrow gain line PRO, the role of the diaphragm is only to remove the high-order rings associated with the higher-order longitudinal modes, but not to influence the central ring. The soliton width, e.g., is given here by the width of the

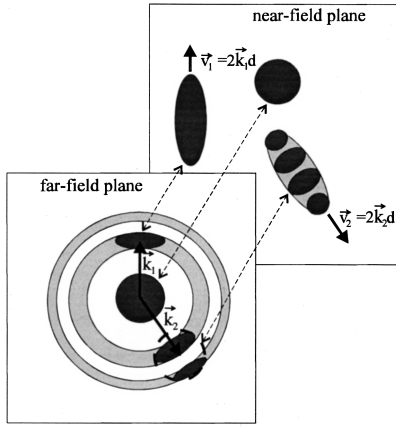


FIG. 2. Intensity distributions in the near and the far field. A central spot in the far field corresponds to an arbitrarily positioned stationary soliton in the near field. A spot on a resonant ring ( $\vec{k}_1 \neq \vec{0}$ ) corresponds to a moving soliton. Emission involving two (or more) resonant rings ( $\vec{k}_2$ ) corresponds to moving solitons, which are modulated along the direction of propagation.

central spot or the thickness of the ring in the far field, in other words, by the gain line width, and not by the diaphragm radius.

### III. SATURABLE ABSORBER IN THE FOURIER-CONJUGATED PLANE

At relatively high pump intensities (20–30 mW/cm<sup>2</sup>) a speckle structure is observed in the near field. The absorber is completely saturated, thus the system behaves like a laser. However, decreasing the pump intensity unsaturates the absorber and only the most intense spots from the disordered patterns remain, forming solitons. The number of solitons drops with pump and finally only one soliton remains, located arbitrarily in the cross section of the saturable absorber. In the far-field plane the corresponding spot is centered around the optical axis of the system ( $\vec{k}_\perp^2 \approx 0$ ) if the resonator detuning is zero. This case is illustrated by the central spot in Fig. 2.

The stationary soliton is analogous to those in [1–3], except for its dependence on the detuning: The solitons decay for negative resonator detuning (for  $l > 0$ ). The solitons can then be excited again only after another exposure of the BR absorber to the bleaching light and at zero detuning.

For positive detuning, the solitons become nonstationary: Depending on the detuning value, the solitons splits into two or three dynamical solitons moving in different directions. The typical experimentally observed soliton dynamics at relatively small resonator detuning (visible as a slight broadening of the central spot in the far-field plane) is shown in Fig. 3. One soliton splits into two, which move in opposite directions. One of them “dies,” e.g., due to larger losses near the edge of the aperture. The other survives, splits again, and this process repeats periodically.

For a theoretical analysis of moving solitons the model equation [1] has to be modified. Taking into account the saturable absorber, like in [2], one obtains

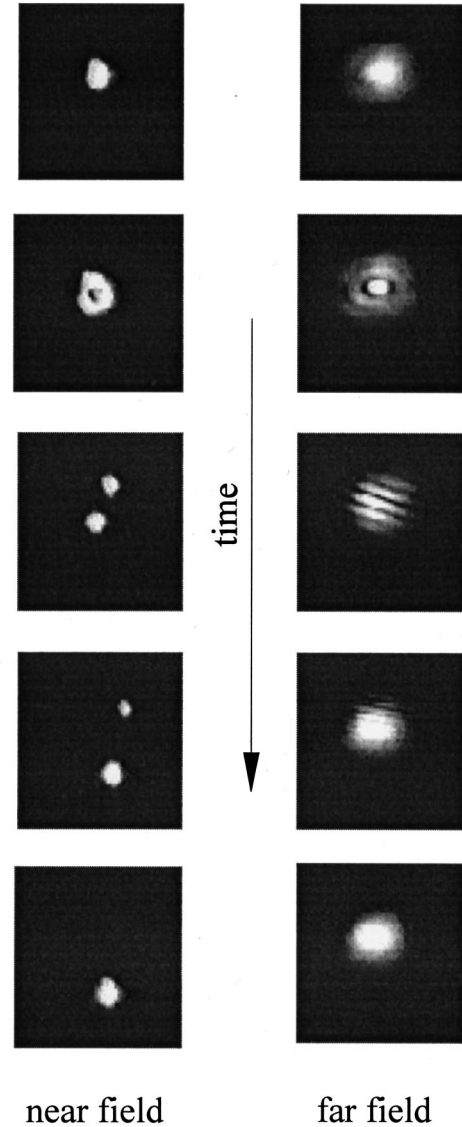


FIG. 3. Experimental observation of soliton dynamics in the near and the far field when only one resonant ring is allowed. Detuning is around 20% of the free spectral range. The time interval between adjacent pictures is 6 s.

$$\begin{aligned} \partial A / \partial t = & -A + i(\Delta + d\vec{\nabla}_\perp^2)A - \frac{(\Delta + d\vec{\nabla}_\perp^2)^2}{\Delta\omega^2} A - \hat{N}(\alpha, I_\alpha)A \\ & + \hat{F}^{-1}\hat{N}(p, I_p)\hat{F}A. \end{aligned} \quad (2)$$

Here the definitions of the parameters remain as in Eq. (1).  $\hat{N}(\alpha, I_\alpha)$  is a nonlinear operator

$$\hat{N}(\alpha, I_\alpha)A = \frac{\alpha A}{1 + |A|^2 / I_\alpha}. \quad (3)$$

The operator of saturable absorption  $\hat{N}(\alpha, I_\alpha)$  acts on the field variable  $A(\vec{r}_\perp, t)$  in the spatial domain (near-field plane) ( $I_\alpha$  is the field intensity saturating the absorber). The

gain occurs in the far-field plane, thus the nonlinear gain operator acts on the field in the Fourier domain ( $p$  is the unsaturated gain and  $I_p$  is the gain saturation intensity). The spatial Fourier transform (and inverse Fourier transform) is therefore used in Eq. (2) to change from the near-field to the far-field domain (and vice versa):

$$\hat{F}A = \frac{1}{2\pi} \int \int A(x, y, t) \exp(ik_x x + ik_y y) dx dy, \quad (4a)$$

$$\hat{F}^{-1}A = \frac{1}{2\pi} \int \int A(k_x, k_y, t) \exp(-ik_x x - ik_y y) dk_x dk_y. \quad (4b)$$

The spatial coordinate in the far-field plane is related to the transverse wave number by  $r_F = k_\perp (\lambda f / \pi)$ . (A Gaussian beam of width  $r_0 = \sqrt{\lambda f / \pi}$  is of the same width in the near- and far-field planes of a self-imaging resonator with lenses with focal length  $f$ .)

Numerical integration of Eq. (2) leads to moving solitons (Fig. 4), similar to those observed experimentally (Fig. 3). Figure 4 illustrates a permanent process of formation of two moving solitons in the case of a small, positive detuning. The scenario starts from the splitting of one soliton into two solitons moving in opposite directions. Due to periodic boundary conditions used in the numerical integration, the motion of both solitons can last relatively long, until they finally (accidentally) collide. In the collision process one of two solitons dies and the process described above repeats.

To interpret the moving solitons, let us assume that a radiation spot appears on the ring, centered around a particular resonant wave number  $\vec{k}_\perp = (k_x, 0)$ ,  $dk_x^2 = \Delta$  (this case is also illustrated in Fig. 2). This off-central spot corresponds in the near-field plane to a soliton moving with a particular velocity, dependent on  $\vec{k}_\perp$ , and directed along the  $x$  axis. To show the motion of the soliton we rewrite the amplitude equation (2) using a planform of the tilted wave with the wave vector  $\vec{k}_\perp$ ,  $A(\vec{r}_\perp, t) = B(\vec{r}_\perp, t) \exp(ik_x x)$ :

$$\begin{aligned} \partial B / \partial t = & -B + id(\vec{\nabla}_\perp^2 + 2ik_x \partial / \partial x)B - \frac{d^2(\vec{\nabla}_\perp^2 + 2ik_x \partial / \partial x)^2}{\Delta \omega^2} B \\ & - \hat{N}(\alpha, I_\alpha)B + \hat{F}^{-1} \hat{N}(p, I_p) \hat{F}B. \end{aligned} \quad (5)$$

The nonlinear operators are invariant with respect to the multiplier  $\exp(ik_x x)$ . [The multiplier  $\exp(ik_x x)$  corresponds to a coordinate shift in the Fourier domain:  $A(\vec{k}_\perp, t) = B(\vec{k}_\perp - \vec{k}_x, t)$ .] Assuming large spatial scales  $\partial_x, \partial_y \ll k_x$ , Eq. (5) can be rewritten

$$\begin{aligned} (\partial / \partial t + 2dk_x \partial / \partial x)B = & -B + id\vec{\nabla}_\perp^2 B \\ & + \frac{d^2(4k_x^2 \partial^2 / \partial x^2 - \partial^4 / \partial y^4)}{\Delta \omega^2} B \\ & - \hat{N}(\alpha, I_\alpha)B + \hat{F}^{-1} \hat{N}(p, I_p) \hat{F}B, \end{aligned} \quad (6)$$

which means that (i) the envelope  $B(\vec{r}_\perp, t)$  propagates with a constant group velocity  $v = 2dk_x = 2\sqrt{d\Delta}$  along the direction of the tilted wave (using hydrodynamical terminology, it is

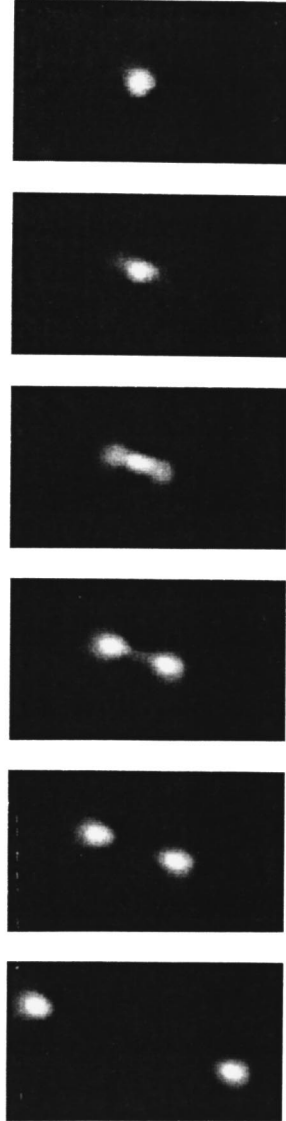


FIG. 4. Dynamics of solitons as obtained by numerical integration of Eq. (2). Time runs from top to bottom; the interval between the plots is  $\Delta t = 6$  (except for the last plot, where  $\Delta t = 18$ ). The parameters are  $\Delta = 1$ ,  $d = 0.25 \times 10^{-3}$ ,  $\Delta \omega = 2$ ,  $p = 2.6$ ,  $I_p = 10$ ,  $\alpha = 2$ , and  $I_\alpha = 0.25$ . The integration region is of unit size. (Only half of the integration region is shown.)

advected by the underlying tilted wave) and (ii) the envelope diffusion is anisotropic with respect to the direction of propagation of the underlying tilted wave: Diffusion is stronger along the direction of propagation (along  $k_x$ ) and weaker in the perpendicular direction.

Larger detuning leads to emission on a resonant ring of larger diameter. Figure 5 shows the numerically calculated multiple solitons and the spatial Fourier spectrum for detuning larger than that corresponding to Fig. 4. We note that the moving solitons are stretched along the direction of motion. The motion direction can be traced from the phase plot since it coincides with the direction of the phase gradient.

As the individual solitons compete for the gain, more moving solitons can exist simultaneously on rings of larger radius. Thus, in general, the faster solitons coexist better.

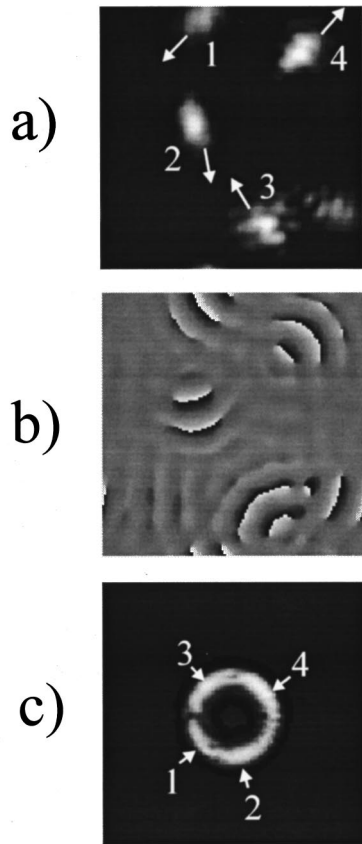


FIG. 5. Dynamical solitons as obtained by numerical integration of Eq. (2): (a) intensity, (b) phase, and (c) spatial Fourier spectrum. The phase gradients indicate the direction of motion. The parameters are as in Fig. 4, except for detuning:  $\Delta = 3$ .

#### IV. BEYOND THE SINGLE LONGITUDINAL MODE APPROACH

In the experiment we could observe soliton dynamics also beyond that described by model (2). Model (2) assumes a single longitudinal mode; thus only one resonant ring can be present in the Fourier domain. In experiments multiple resonant rings are possible if the diaphragm is opened. In Fig. 6(a) three different solitons, with three different directions and velocities of motion corresponding to three different resonant rings, are simultaneously present (one ring is actually degenerated to the central spot here). The dynamical solitons can coexist if they move with different velocities or in different directions. Otherwise they overlap and compete for the common gain in the far-field plane. The velocity modulus and direction of motion correspond to the field distribution in the far field (see Fig. 2 for illustration).

Figure 6(b) shows three solitons moving with equal velocity modulus but in different directions (belonging to the same resonant ring). The moving solitons coexist with a stationary one. Figure 6(c) shows the spatially modulated dynamical solitons, which in the far-field domain correspond to the simultaneous emission on two (or more) resonant rings. This situation is also not describable by the “single-longitudinal-mode” model.

#### V. CONCLUSIONS

Stationary solitons corresponding to emission on the central spot in the far field can move freely in the near field. As

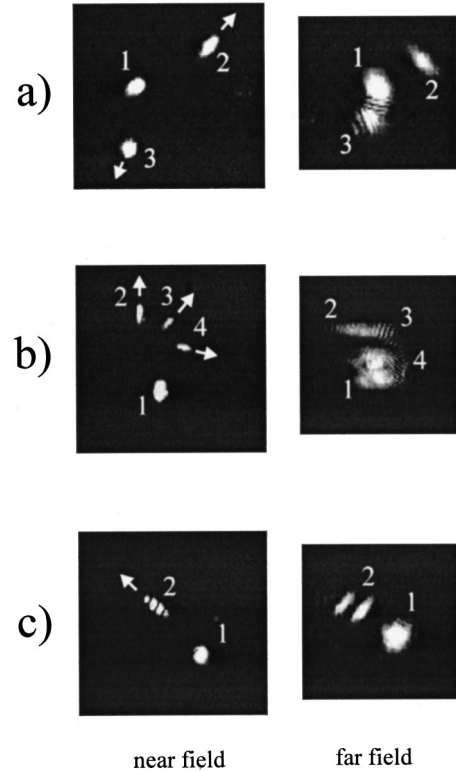


FIG. 6. Experimental observation of moving solitons in the near- and far-field domains, corresponding to a simultaneous presence of a few resonant rings. Stationary solitons (1) and two dynamical solitons corresponding to the first and second resonant rings (2 and 3) are shown in (a). Three solitons moving with equal velocity modulus, coexisting with stationary soliton, are shown in (b). A spatially modulated moving soliton, corresponding to simultaneous emission on a few resonant rings, is shown in (c).

they compete for the gain, only one stationary soliton exists. The direction of motion of the moving solitons is free. Moving solitons correspond to emission of part of a far-field ring. The velocity modulus depends on the resonator detuning. (By changing the resonator length, one can continuously change the velocity of the solitons or stop the motion.)

The moving solitons are stretched along the direction of propagation (or equivalently occupy elongated sectors on the resonant rings). Mathematically, the stretching is related to the anisotropic diffusion with respect to the direction of propagation (or the direction of the underlying tilted wave).

Solitons moving at the same velocity but in different directions coexist because they occupy nonoverlapping fractions of a far-field ring. Solitons with a different modulus of velocity also coexist because they correspond to the different longitudinal modes of the resonator (different rings in the far field). The solitons compete in velocity space and only one soliton can occupy a given velocity (momentum) state.

#### ACKNOWLEDGMENTS

This work has been supported by ESPRIT LTR Project “PASS,” Deutsche Forschungsgemeinschaft under Grant No. We-743/8-2, Volkswagen Stiftung, and BMFT under Grant No. X272.4.

- [1] V. Yu. Bazhenov, V. B. Taranenko, and M. V. Vasnetsov, *Proc. SPIE* **1840**, 183 (1992).
- [2] V. B. Taranenko, K. Staliunas, and C. O. Weiss, *Phys. Rev. A* **56**, 1582 (1997).
- [3] M. Saffman, D. Montgomery, and D. Z. Anderson, *Opt. Lett.* **19**, 518 (1994).
- [4] K. Staliunas, M. F. H. Tarroja, G. Slekyš, C. O. Weiss, and L. Dambly, *Phys. Rev. A* **51**, 4140 (1995).
- [5] K. Staliunas, *Phys. Rev. A* **48**, 4847 (1993); K. Staliunas and C. O. Weiss, *Physica D* **81**, 79 (1985).
- [6] J. Lega, J. V. Moloney, and A. C. Newell, *Phys. Rev. Lett.* **73**, 2978 (1994).
- [7] S. Longhi, and A. Geraci, *Phys. Rev. A* **54**, 4581 (1996).
- [8] V. Yu. Bazhenov, M. S. Soskin, V. B. Taranenko, and M. V. Vasnetsov, in *Optical Processing and Computing* (Academic, Boston, 1989), p. 103; N. Hampp, C. Brauchle, and D. Oesterhelt, *Biophys. J.* **58**, 83 (1990); R. R. Birge, *Annu. Rev. Phys. Chem.* **41**, 683 (1990).
- [9] K. Staliunas, G. Slekyš, and C. O. Weiss, *Phys. Rev. Lett.* **79**, 2658 (1997).
- [10] P. K. Jakobsen, J. V. Moloney, A. C. Newell, and R. Indik, *Phys. Rev. A* **45**, 8129 (1992).